PHOTOREACTIONS CREATE SUPERCONDUCTING MATERIALS

Yulun Han and Dmitri Kilin[*]

UDC 537.312.62

One of the potentially transformative areas of scientific development is to achieve superconductivity at room temperature. Recently, the photochemical synthesis was carried out to prepare carbonaceous sulfur hydride (CSH) systems with room-temperature superconductivity at high pressure. In this work, we present a first-principles study aiming to unravel the photoreaction of sulfur with molecular hydrogen using the time-dependent excited-state molecular dynamics (TDESMD) methodology. Individual TDESMD trajectory provides details about reactions that lead to a number of allotropes of sulfur and their hydrogenated forms. Simulated mass spectra based on an ensemble of TDESMD trajectories provide the distribution of sulfanes along reaction pathways. It is found that the photoreaction starts with ring opening of cyclic S_8, which may then react with two H radicals to form S_8H_2 as a result of the homolytic dissociation of H_2. The sulfur cluster will undergo the elimination of small fragments, which can later recombine into a variety of sulfanes. The most abundant fragments generated along trajectories are H_2S, S_4H_2, and S_8H_2. The final sulfur-bearing products are a mixture of sulfanes with various chains and rings. The mechanistic and conformational information obtained from this work allows us to better understand the photoreaction, and potentially, give insights into the preparation of high T_c materials using similar reactants.

Keywords: photochemical synthesis, superconductivity, TDESMD methodology.

Introduction. One of the potentially transformative areas of scientific development is to achieve superconductivity at room temperature. In the past few years, hydrogen rich materials with high superconducting transition temperature (T_c) under high pressure have attracted much attention [1–7]. The superconductivity of these materials is realized as a result of high-frequency phonon modes and strong electron–phonon coupling provided by the light mass of hydrogen [8–10]. A recent experimental work reported a T_c of 288 K in a carbonaceous sulfur hydride system (C–S–H) at 267 GPa [11]. This material was photosynthesized by combining elemental carbon and sulfur with molecular hydrogen at 4 GPa. The proposed reaction pathways started with the photoscission of S–S bonds of elemental sulfur, giving rise to S free radicals, which then reacted with H_2 to form H_2S [11, 12]. The synthesized compound was suggested to be a mixed alloy of H_2S and CH_4 with stoichiometry $(CH_4)_x(H_2S)_{2-x}H_2$ [11]. To evaluate the plausibility of experimentally proposed reaction pathways and to clarify microscopic structures of products for individual reaction steps, it is necessary to conduct theoretical studies on the photoreaction.

Ab initio molecular dynamics (AIMD) simulations are indispensable tools to reveal a mechanistic picture of reaction events, which is difficult to deduce from experiments. Modeling the photoreactions requires careful consideration of strong coupling between electronic and vibrational degrees of freedom and thus remains elusive, as opposed to modeling the ground-state chemical processes. To include electronic excited-state effects in the AIMD simulations, various approaches going beyond the Born–Oppenheimer approximation have been developed with different levels of electronic structure calculations [13–16]. A representative example is nonadiabatic excited state molecular dynamics (NEXMD), which has been used to describe photoinduced phenomena in organic conjugated materials [17–20]. Over the years, our group has developed a time-dependent excited-state molecular dynamics (TDESMD) algorithm using a combination of Rabi theory [21, 22] and surface hopping approximations [23–25] to model photofragmentation, photodimerization, and photocatalysis for systems ranging from small organic [26] and inorganic molecules [27] to metal–organic complexes [28–30] and to periodic carbon nanotubes [31].

---

[*]To whom correspondence should be addressed.

North Dakota State University, Department of Chemistry and Biochemistry, Fargo, USA; email: dmitri.kilin@ndsu.edu.

Inspired by [11], we present a first-principles study aiming to unravel the photoreaction of elemental sulfur with molecular hydrogen using the TDESMD methodology. Individual TDESMD trajectory provides details about reactions that lead to a number of allotropes of sulfur and their hydrogenated forms. Simulated mass spectra based on an ensemble of TDESMD trajectories provide the distribution of sulfanes along reaction pathways. The mechanistic and conformational information obtained from this work allows us to better understand the photoreaction, and potentially, give insights into the preparation of high T_c materials using similar reactants.

Methods. All calculations are carried out using DFT on the basis of Kohn–Sham (KS) orbitals within the Vienna *Ab initio* Simulation Package (VASP) [32–36]. The generalized gradient approximation (GGA) [37, 38] for the exchange-correlation functional of Perdew–Burke–Ernzerhof (PBE) [38] is adopted. The projected augmented wave (PAW) [39] potentials on a plane-wave basis are used. A plane-wave energy cutoff is set as 500 eV. The dispersion interactions are treated with the semiempirical atom pairwise corrections known as DFT-D3 by Grimme et al. [40]. The Brillouin zone is only sampled at the gamma point. The external pressures are enforced by the stress tensor (PSTRESS keyword). The absorption spectra are calculated by adopting independent orbital approximations (IOAs) [41]. Each TDESMD trajectory is performed up to 2.5 ps using a time step of 1 fs with an inverse Rabi frequency of 10 fs. The reaction intermediates and products generated along TDESMD trajectories possess nonzero kinetic energy. In the late stages of trajectories, the accumulated thermal energy is considerable. Thus, one observes exaggerated bond elongation and contraction for reaction products, which prevents further analysis in structure–property relationship. One strategy to solve the problem of structural ambiguity is to relax the reaction intermediates and products upon cooling through thermal energy dissipation. Note that the cooling is a postprocessing computational technique and the relaxed intermediates and products are not introduced back to TDESMD trajectories. Mass spectra are extracted from the relaxed intermediates and products along TDESMD trajectories based on Python compatible cheminformatics program Open Babel [42]. The interatomic distance is used to determine the number of fragments and number of nuclei in each fragment. Atomic models are visualized using VESTA software [43].

Results and Discussion. Elemental sulfur can exist in a variety of allotrope forms [44]. In this work, we consider the most common allotrope S_8 with well-known ring structure, which is extracted from the crystal structure of α-S phase [45]. There are two atomic models: one with 24 H_2 molecules and the other with 16 H_2 and 8 CH_4 molecules surrounding S_8. Figure 1a–d shows the optimized structures of S_8 with H_2 and $H_2 + CH_4$ at 4 GPa. The external pressure is assigned to match the experimental conditions [11]. These geometry optimized models serve as starting points for the simulation of photochemistry through TDESMD calculations. We explore the structural response of atomic models to external pressures by allowing the unit cell parameters and nuclear positions to fully relax at the specified pressure value. The values of total energy and cell volume for S_8 with H_2 and $H_2 + CH_4$ under various external pressures are plotted in Fig. 1e. With increasing external pressure, the total energy increases while the cell volume decreases.

Figure 1f,g shows the basic electronic structure of the initial configuration of reactant cells before irradiation. There are similarities in DOS and absorption spectra of these cells, since frontier orbitals are localized on sulfur rings. In the absorption spectra, the intense transitions (a–e) and (a′–c′) with high oscillator strengths are used as initial excitation conditions for TDESMD calculations for S_8 with H_2 and with $H_2 + CH_4$, respectively.

The influence of laser field is explicitly considered in TDESMD simulations, which introduces time-dependent perturbations leading to transitions between excited and ground states. The excitation energy is redistributed into nuclear kinetic energy, facilitating the exploration of dissociation channel of the reaction. The procedure for the TDESMD algorithm focusing on the coupled electronic and nuclear trajectory under the influence of light has been described in detail [29]. Figure 2 shows representative snapshots along the TDESMD trajectory with electrons hopping between the orbital pair (HOMO-3, LUMO) for elemental S_8 with H_2 at 4 GPa. In the early stages of the trajectory, the ring structure of S_8 is intact and experiences only the elongation and contraction of S–S bonds. Subsequently, one observes the breaking (Fig. 2a) and reformation of S-S bonds as a result of increasing kinetic energy. Meanwhile, most of H_2 molecules serve as non-participating spectators. After ∼610 fs, the collision-induced cleavage of H–H bond for one H_2 molecule in close proximity to S_8 is observed, leading to the formation of a dihydrogen bonded (–S–H···H–S–) sulfur cluster (Fig. 2b–d). We conduct Bader charge analysis [46–48] to explore the nature of the H_2 dissociation. The heterolytic dissociation typically requires the strong polarization of H_2, which facilitates the formation of a tight ion pair, and finally entails the formation of a hydride and a proton with well-identified Bader charges. In contrast, one finds the H Bader charges of ±0.09 e for the structure in Fig. 2b, indicating that the H–H bond is slightly polarized. For structures in Fig. 2c,d it is found that H Bader charges decrease slightly. Therefore, the H_2 dissociates through the homolytic pathway, which produces two radicals that combine with elemental sulfur.
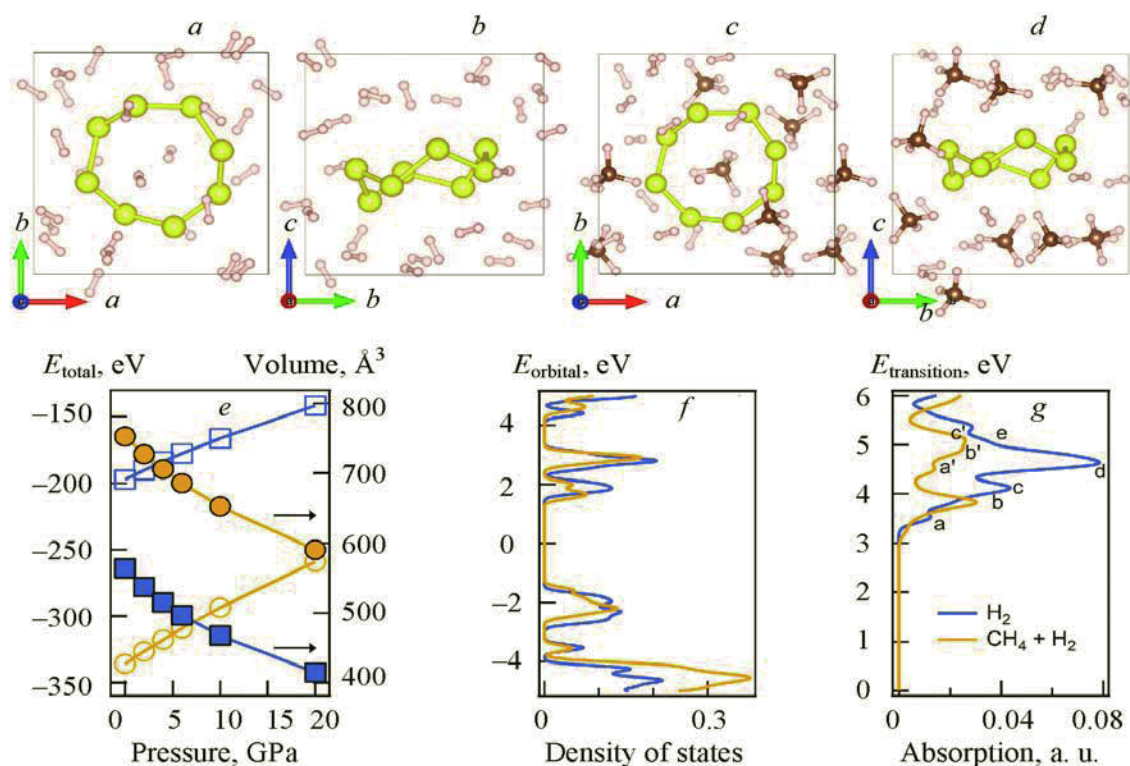
Fig. 1. Various views of optimized structures of S_8 with (a, b) H_2 and (c, d) H_2 + CH_4 at 4 GPa, (e) total energy (open symbols) and atomic cell volume (filled symbols) as a function of external pressure for H_2 (squares) and H_2 + CH_4 (circles), (f) DOS and (g) calculated absorption spectra of optimized structures of S_8 with H_2 and H_2 + CH_4 at 4 GPa.

Following the hydrogenation, the cluster undergoes cracking through the elimination of S_2 and S_2H. The ejected fragments are then recaptured, giving rise to the S_8H_2 cluster with the loss of the dihydrogen bond (Fig. 2e). Note that the ejection and recapture of small sulfur fragments are abundant in the remaining trajectory because of the considerable thermal energy. After ~760 fs, one hydrogen atom in the cluster is found to be labile. As a result, one observes the hydrogen migration to the SH group, forming a neutral H_2S molecule (Fig. 2f,g). The H_2S molecule remains unbound and is stable for ~350 fs. After ~1300 fs, one H atom of H_2S migrates back to the S_7 cluster, leading to a S_7H cluster with a S_4 cyclic structure and a S_3H group (Fig. 2h). In final stages of the trajectory, the sulfur S_6 skeleton is preserved, while the SH group in the chain can be ejected and recombine with the free SH group to form a neutral H_2S_2 molecule (Figs. 2i–l). Meanwhile, one also observes that more H_2 molecules participate in the reaction. There are subsequent homolytic dissociation of two H_2 molecules (H3–H4 and H5–H6). The resulting radicals H3 and H5 are captured by sulfur, while H4 and H6 recombine to form a H_2 molecule. For the final product two more H_2 (H7–H8 and H9–H10) molecules are in short contact with the sulfur chain. Together with other trajectories, we find the photoreaction starts with ring opening of S_8, which may then react with H_2 to form S_8H_2. S_8 or S_8H_2 cluster will undergo the elimination of small fragments, which can later recombine into different chain and cyclic structures and be hydrogenated. It is worth noting that the final sulfur-bearing products are not H_2S molecules as reported in experiments [11] but a mixture of sulfanes.

Figure 3a shows the energy diagram of relaxed intermediates and products along the TDESMD trajectory with electrons hopping between the orbital pair (HOMO-3, LUMO) for elemental S_8 with H_2 at 4 GPa. We identify nine representative reaction products in the energy diagram. For the first half of the trajectory, the dominant structure is **1**, S_8 ring, which is similar to the initial reactant. The homolytic dissociation of H_2 leads to a local minimum corresponding to structure **2**, open-chain S_8H_2 in which the terminal S atoms are hydrogenated. Structure **2** dissociates to **3**, H_2S and seven-membered S_7 ring due to the hydrogen migration, as illustrated in the second row of Fig. 2. Also, structure **3** is not far in energy from structure **1**. Recapture of H_2S by the sulfur cluster leads to a local maximum corresponding to structure **4**,
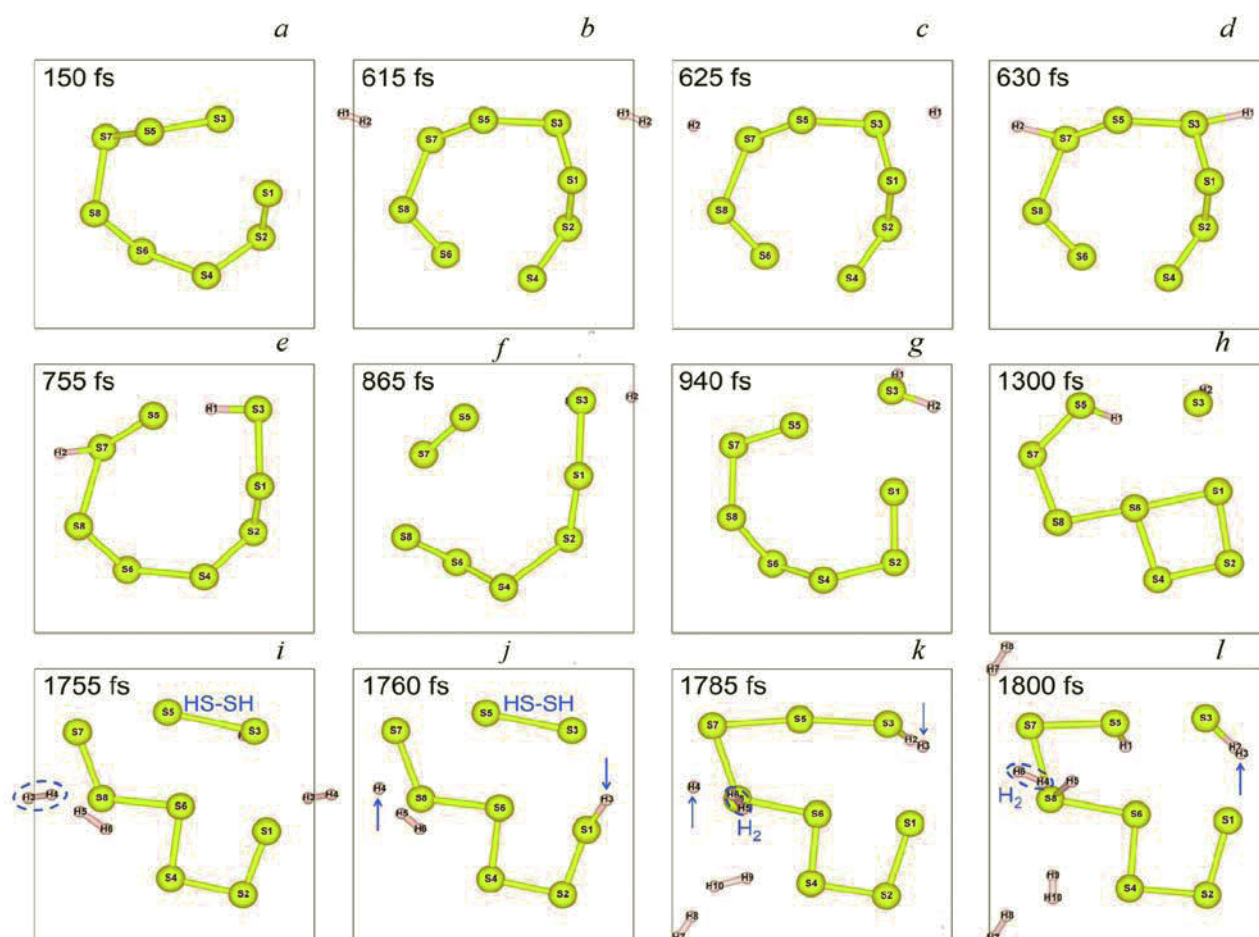
641

Fig. 2. Snapshots along the TDESMD trajectory with electrons hopping between the orbital pair (HOMO-3, LUMO) for elemental S8 with H_2 at 4 GPa. The nonparticipating spectator H_2 molecules are not shown for clarity.

open-chain S_8H_2 in which H_2S is attached to the S_7 chain. Later in the trajectory, H_2S is ejected and one free H_2 molecule is in proximity to the sulfur cluster for a short period of time. The relaxation during this period leads to a local minimum corresponding to structure **5**, H_2S and hydrogenated open-chain S_7H_2. When this free H_2 molecule stays away from the sulfur cluster, the relaxation produces structure **6**, H_2S, S_2, and S_5. A more stable structure is obtained for structure **7**, H_2S and open-chain S_7, as the eclipsed S_4 chain transforms into cyclic ring and S_2 recombines with S_5 chain. In the second half of the trajectory, the dominant structure is **8**, open-chain S_6 and a stack of two SH as a result of hydrogen migration from H_2S to the S_7 cluster. As more H_2 molecules are involved in the reaction through homolytic dissociation or hydrogen bonding, the final product **9** forms a stable framework consisting of cyclic S_4H ring, 3 SH, H_2S, and H_2, where most of sulfur atoms are on the (001) plane for structure **9**.

We then explore the electronic properties of structures **1**–**9**. It is found that the band gaps remain open for all structures (Fig. 3b). Interestingly, the band gaps almost decrease for metastable intermediates as the reaction proceeds. Note structures **5** and **9** are local energy minima and more H_2 molecules are involved for the formation of these structures than others. The band gaps for structure **1**, structure **4** (intermediate with the highest energy), and structure **9** are ~3.2, 1.3, and 2.0 eV, respectively. The charge density analysis indicates that structure **9** should be considered as an isolated fragment instead of a polymeric chain. The nonzero band gap for the product **9** is not surprising, considering it has similarity to the van der Waals solids responsible for superconductivity, but not the same. To produce correct product, the simulations need to account relativistic and spin–orbit coupling (SOC) effects in a perturbative way and enable collective excitations beyond the single-determinant method.
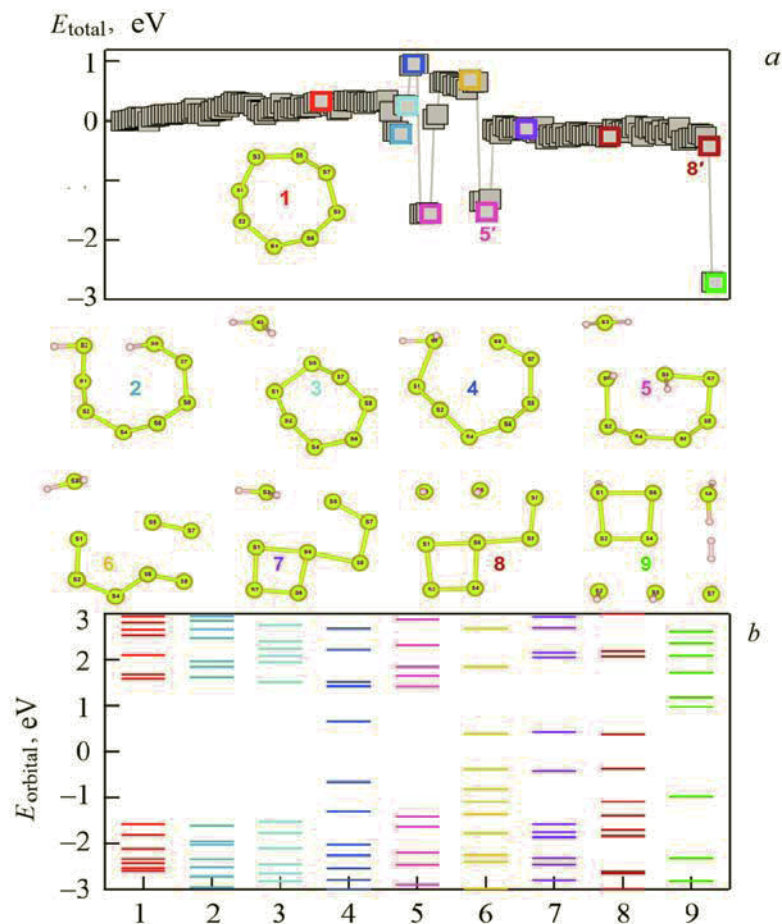
Fig. 3. (a) Energy diagram of relaxed reaction intermediates and products extracted from the TDESMD trajectory with electrons hopping between orbital pair (HOMO-3, LUMO) for elemental S_8 with H_2 at 4 GPa. Structures **5′** and **8′** are similar to structures **5** and **8**, respectively, (b) energy levels for representative intermediates. The non-participating spectator H_2 molecules are not shown for clarity.

Figure 4 shows the simulated mass spectra based on relaxed intermediates and products from TDESMD trajectories. Here, we only focus on sulfur-containing fragments. In the mass spectra, there are eight groups of fragments from S_8 to S_1. Within each group there are several peaks, each corresponding to a fragment with the same number of sulfur atoms but differing numbers of hydrogen atoms. In some trajectories, the structural relaxation of intermediates leads to polymeric sulfur chains. These fragments have indefinite molecular weights and represent less than 2% of the total amount, and thus are left out of the computed mass spectra. In Fig. 4, the dominant feature is S_8, since it takes considerable time to accumulate thermal energy to facilitate the cracking of S_8 ring structure. Furthermore, it is found that occurrences of fragments containing up to two bound hydrogen atoms are abundant. Fragments with more than two bound hydrogen are not observed, except for S_3, S_4, and S_8 groups, all of which are characterized with low occurrences. The mass spectra from H_2 and $H_2 + CH_4$ are similar, because methane molecules serve as nonparticipating spectators throughout the simulation. A minor discrepancy of intensities of fragments is observed between the two spectra with and without methane. Specifically, in each of S_1–S_7 groups the most abundant fragment is the hydrogenated form of sulfur allotrope, except for S_6 in case of H_2 and S_3 in case of $H_2 + CH_4$. The mass spectrum from H_2 shows stronger intensities for S_1–S_7 groups but weaker intensities for the S_8 group than the spectrum from $H_2 + CH_4$. The discrepancy originates from inconsistent numbers of atoms in simulation cells, as the redistribution of thermal energy is more efficient for a smaller cell with fewer atoms.
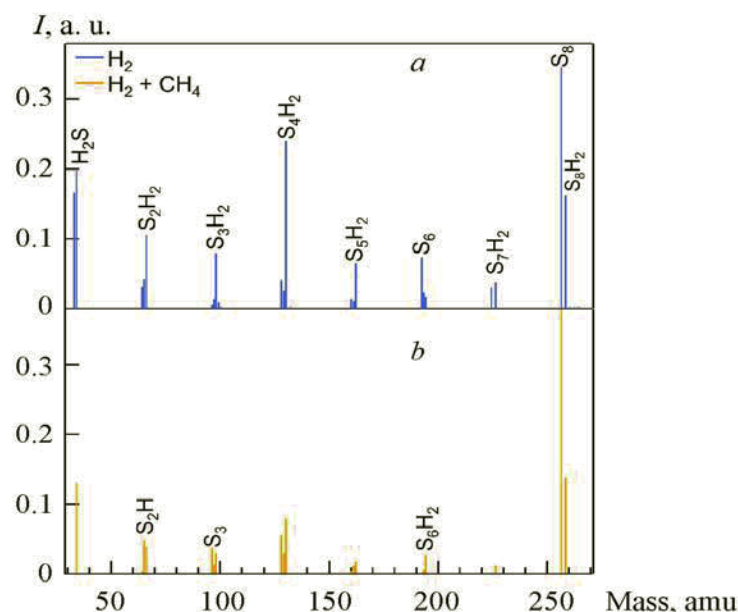
643

Fig. 4. Simulated mass spectra from TDESMD trajectories for elemental S_8 with H_2 (a) and with $H_2 + CH_4$ (b) at 4 GPa. For each spectrum, one divides the number of fragments with the same composition by the total number of fragments to calculate the normalized intensity.

Conclusions. TDESMD calculations are carried out to simulate photoinduced reactions of cyclic S_8 with H_2 or $CH_4 + H_2$ at pressure of 4 GPa. In the latter case, S_8 and H_2 molecules serve as reactants, while CH_4 molecules serve as nonparticipating spectators. From a set of nuclear configurations formed at subsequent instants of time, we observe several reaction steps leading to a number of allotropes of sulfur and their hydrogenated forms. It is found that the photoreaction starts with ring opening of S_8, which may then react with two H radicals to form S_8H_2 as a result of the homolytic dissociation of H_2. The sulfur cluster will undergo the elimination of small fragments, which can later recombine into a variety of sulfanes. Along the trajectories, one observes the appreciable abundance of hydropolysulfides S_xH_2 ($x = 1$–8). The most abundant fragments generated in the reactions are H_2S, S_4H_2, and S_8H_2. The final sulfur-bearing products are a mixture of sulfanes with various chains and rings. The findings of low-energy configurations are expected to facilitate the efficient exploration of the potential energy surface and avoid exhaustive trial-and-error and guess-and-check processes for searching important reaction pathways. The TDESMD methodology along with mechanistic and conformational information obtained from this work are applicable to similar reactants, which potentially contribute to the photochemical synthesis of high T_c materials.

REFERENCES

1. A. P. Drozdov, M. I. Eremets, I. A. Troyan, V. Ksenofontov, and S. I. Shylin, *Nature*, **525**, 73–76 (2015).
2. A. P. Drozdov, P. P. Kong, V. S. Minkov, S. P. Besedin, M. A. Kuzovnikov, S. Mozaffari, L. Balicas, F. F. Balakirev, D. E. Graf, V. B. Prakapenka, et al., *Nature*, **569**, 528–531 (2019).
3. M. Somayazulu, M. Ahart, A. K. Mishra, Z. M. Geballe, M. Baldini, Y. Meng, V. V. Struzhkin, and R. J. Hemley, *Phys. Rev. Lett.*, **122**, Article ID 027001 (2019).
4. I. Errea, F. Belli, L. Monacelli, A. Sanna, T. Koretsune, T. Tadano, R. Bianco, M. Calandra, R. Arita, F. Mauri, et al., *Nature*, **578**, 66–69 (2020).

5. L. Zhang, Y. Wang, J. Lv, and Y. Ma, *Nature Rev. Mater.*, **2**, Article ID 17005 (2017).

6. M. I. Eremets, I. A. Trojan, S. A. Medvedev, J. S. Tse, and Y. Yao, *Science*, **319**, 1506–1509 (2008).

7. Y. Sun, J. Lv, Y. Xie, H. Liu, and Y. Ma, *Phys. Rev. Lett.*, **123**, Article ID 097001 (2019).

8. N. W. Ashcroft, *Phys. Rev. Lett.*, **21**, 1748–1749 (1968).

9. N. W. Ashcroft, *Phys. Rev. Lett.*, **92**, Article ID 187002 (2004).

10. J. A. Flores-Livas, L. Boeri, A. Sanna, G. Profeta, R. Arita, and M. Eremets, *Phys. Rep.*, **856**, 1–78 (2020).

11. E. Snider, N. Dasenbrock-Gammon, R. McBride, M. Debessai, H. Vindana, K. Vencatasamy, K. V. Lawler, A. Salamat, and R. P. Dias, *Nature*, **586**, 373–377 (2020).

12. B. Eckert, R. Schumacher, H. J. Jodl, and P. Foggi, *High Pressure Res.*, **17**, 113–146 (2000).

13. J. C. Vincent, M. Muuronen, K. C. Pearce, L. N. Mohanam, E. Tapavicza, and F. Furche, *J. Phys. Chem. Lett.*, **7**, 4185–4190 (2016).

14. S. M. Parker, S. Roy, and F. Furche, *Phys. Chem. Chem. Phys.*, **21**, 18999–19010 (2019).

15. C. Cisneros, T. Thompson, N. Baluyot, A. C. Smith, and E. Tapavicza, *Phys. Chem. Chem. Phys.*, **19**, 5763–5777 (2017).

16. M. Muuronen, S. M. Parker, E. Berardo, A. Le, M. A. Zwijnenburg, and F. Furche, *Chem. Sci.*, **8**, 2179–2183 (2017).

17. Y. Zhang, L. Li, S. Tretiak, and T. Nelson, *J. Chem. Theory Comp.*, **16**, 2053–2064 (2020).

18. A. E. Sifain, B. J. Gifford, D. W. Gao, L. Lystrom, T. R. Nelson, and S. Tretiak, *J. Phys. Chem. A*, **122**, 9403–9411 (2018).

19. W. Malone, B. Nebgen, A. White, Y. Zhang, H. Song, J. A. Bjorgaard, A. E. Sifain, B. Rodriguez-Hernandez, V. M. Freixas, S. Fernandez-Alberti, et al., *J. Chem. Theory Comp.*, **16**, 5771–5783 (2020).

20. L. Lystrom, Y. Zhang, S. Tretiak, and T. Nelson, *J. Phys. Chem. A*, **122**, 6055–6061 (2018).

21. I. I. Rabi, *Phys. Rev.*, **51**, 652–654 (1937).

22. I. I. Rabi, N. F. Ramsey, and J. Schwinger, *Rev. Modern Phys.*, **26**, 167–171 (1954).

23. J. C. Tully, *J. Chem. Phys.*, **93**, 1061–1071 (1990).

24. J. C. Tully, *J. Chem. Phys.*, **137**, Article ID 22A301 (2012).

25. S. Hammes-Schiffer and J. C. Tully, *J. Chem. Phys.*, **101**, 4657–4667 (1994).

26. Y. Han, B. Rasulev, and D. S. Kilin, *J. Phys. Chem. Lett.*, **8**, 3185–3192 (2017).

27. Y. Han, K. Anderson, E. K. Hobbie, P. Boudjouk, and D. S. Kilin, *J. Phys. Chem. Lett.*, **9**, 4349–4354 (2018).

28. Y. Han, D. S. Kilin, P. S. May, M. T. Berry, and Q. Meng, *Organometallics*, **35**, 3461–3473 (2016).

29. Y. Han, Q. Meng, B. Rasulev, P. S. May, M. T. Berry, and D. S. Kilin, *J. Chem. Theory Comp.*, **13**, 4281–4296 (2017).

30. Y. Han, Q. Meng, B. Rasulev, P. S. May, M. T. Berry, and D. S. Kilin, *J. Phys. Chem. A*, **119**, 10838–10848 (2015).

31. B. Disrud, Y. Han, and D. S. Kilin, *Mol. Phys.*, **115**, 674–682 (2017).

32. W. Kohn and L. J. Sham, *Phys. Rev.*, **140**, A1133–A1138 (1965).

33. G. Kresse and J. Hafner, *Phys. Rev. B*, **47**, 558–561 (1993).

34. G. Kresse and J. Hafner, *Phys. Rev. B*, **49**, 14251–14269 (1994).

35. G. Kresse and J. Furthmüller, *Phys. Rev. B*, **54**, 11169–11186 (1996).

36. G. Kresse and J. Furthmüller, *Comput. Mater. Sci.*, **6**, 15–50 (1996).

37. J. P. Perdew, J. A. Chevary, S. H. Vosko, K. A. Jackson, M. R. Pederson, D. J. Singh, and C. Fiolhais, *Phys. Rev. B*, **46**, 6671–6687 (1992).

38. J. P. Perdew, K. Burke, and M. Ernzerhof, *Phys. Rev. Lett.*, **77**, 3865–3868 (1996).

39. P. E. Blöchl, *Phys. Rev. B*, **50**, 17953–17979 (1994).

40. S. Grimme, J. Antony, S. Ehrlich, and H. Krieg, *J. Chem. Phys.*, **132**, Article ID 154104 (2010).

41. A. Forde, T. Inerbaev, E. K. Hobbie, and D. S. Kilin, *J. Am. Chem. Soc.*, **141**, 4388–4397 (2019).

42. N. M. O'Boyle, M. Banck, C. A. James, C. Morley, T. Vandermeersch, and G. R. Hutchison, *J. Cheminformat.*, **3**, 33 (2011).

43. K. Momma and F. Izumi, *J. Appl. Crystallogr.*, **44**, 1272–1276 (2011).

44. B. Meyer, *Chem. Rev.*, **64**, 429–451 (1964).

45. S. J. Rettig and J. Trotter, *Acta Crystallogr. C*, **43**, 2260–2262 (1987).

46. W. Tang, E. Sanville, and G. Henkelman, *J. Phys.: Condens. Matter*, **21**, Article ID 084204 (2009).

47. E. Sanville, S. D. Kenny, R. Smith, and G. Henkelman, *J. Comput. Chem.*, **28**, 899–908 (2007).

48. G. Henkelman, A. Arnaldsson, and H. Jónsson, *Comput. Mater. Sci.*, **36**, 354–360 (2006).